World Journal of Gastroenterology

Submit a Manuscript: https://www.f6publishing.com

World J Gastroenterol 2022 August 21; 28(31): 4363-4375

DOI: 10.3748/wjg.v28.i31.4363

ISSN 1007-9327 (print) ISSN 2219-2840 (online)

ORIGINAL ARTICLE

Retrospective Study

Application of computed tomography-based radiomics in differential diagnosis of adenocarcinoma and squamous cell carcinoma at the esophagogastric junction

Ke-Pu Du, Wen-Peng Huang, Si-Yun Liu, Yun-Jin Chen, Li-Ming Li, Xiao-Nan Liu, Yi-Jing Han, Yue Zhou, Chen-Chen Liu, Jian-Bo Gao

Specialty type: Radiology, nuclear medicine and medical imaging

Provenance and peer review: Unsolicited article; Externally peer reviewed.

Peer-review model: Single blind

Peer-review report's scientific quality classification

Grade A (Excellent): A
Grade B (Very good): B, B
Grade C (Good): C
Grade D (Fair): 0
Grade E (Poor): 0

P-Reviewer: Ferreira GSA, Brazil; Ghoneim S, United States; Okasha H, Egypt; Sato H, Japan

Received: March 16, 2022
Peer-review started: March 16, 2022
First decision: June 11, 2022
Revised: June 11, 2022
Accepted: July 25, 2022
Article in press: July 25, 2022
Published online: August 21, 2022

Ke-Pu Du, Wen-Peng Huang, Yun-Jin Chen, Li-Ming Li, Yi-Jing Han, Yue Zhou, Chen-Chen Liu, Jian-Bo Gao, Department of Radiology, The First Affiliated Hospital of Zhengzhou University, Zhengzhou 450052, Henan Province, China

Si-Yun Liu, Department of Pharmaceutical Diagnostics, General Electric Company Healthcare, Beijing 100176, China

Xiao-Nan Liu, Department of Pathology, The First Affiliated Hospital of Zhengzhou University, Zhengzhou 450052, Henan Province, China

Corresponding author: Jian-Bo Gao, PhD, Academic Research, Chairman, Chief Doctor, Instructor, Department of Radiology, The First Affiliated Hospital of Zhengzhou University, No. 1 East Jianshe Road, Zhengzhou 450052, Henan Province, China.
jianbogaochina@163.com

Abstract

BACKGROUND

The biological behavior of carcinoma of the esophagogastric junction (CEGJ) is different from that of gastric or esophageal cancer. Differentiating squamous cell carcinoma of the esophagogastric junction (SCCEG) from adenocarcinoma of the esophagogastric junction (AEG) can indicate Siewert stage and whether the surgical route for patients with CEGJ is transthoracic or transabdominal, as well as aid in determining the extent of lymph node dissection. With the development of neoadjuvant therapy, preoperative determination of pathological type can help in the selection of neoadjuvant radiotherapy and chemotherapy regimens.

AIM

To establish and evaluate computed tomography (CT)-based multiscale and multiphase radiomics models to distinguish SCCEG and AEG preoperatively.

METHODS

We retrospectively analyzed the preoperative contrasted-enhanced CT imaging data of single-center patients with pathologically confirmed SCCEG (n = 130) and AEG (n = 130). The data were divided into either a training (n = 182) or a test group (n = 78) at a ratio of 7:3. A total of 1409 radiomics features were separately

extracted from two dimensional (2D) or three dimensional (3D) regions of interest in arterial and venous phases. Intra-/inter-observer consistency analysis, correlation analysis, univariate analysis, least absolute shrinkage and selection operator regression, and backward stepwise logical regression were applied for feature selection. Totally, six logistic regression models were established based on 2D and 3D multi-phase features. The receiver operating characteristic curve analysis, the continuous net reclassification improvement (NRI), and the integrated discrimination improvement (IDI) were used for assessing model discrimination performance. Calibration and decision curves were used to assess the calibration and clinical usefulness of the model, respectively.

RESULTS

The 2D-venous model (5 features, AUC: 0.849) performed better than 2D-arterial (5 features, AUC: 0.808). The 2D-arterial-venous combined model could further enhance the performance (AUC: 0.869). The 3D-venous model (7 features, AUC: 0.877) performed better than 3D-arterial (10 features, AUC: 0.876). And the 3D-arterial-venous combined model (AUC: 0.904) outperformed other single-phase-based models. The venous model showed a positive improvement compared with the arterial model (NRI > 0, IDI > 0), and the 3D-venous and combined models showed a significant positive improvement compared with the 2D-venous and combined models ($P < 0.05$). Decision curve analysis showed that combined 3D-arterial-venous model and 3D-venous model had a higher net clinical benefit within the same threshold probability range in the test group.

CONCLUSION

The combined arterial-venous CT radiomics model based on 3D segmentation can improve the performance in differentiating EGJ squamous cell carcinoma from adenocarcinoma.

Key Words: Esophagogastric junction; Squamous cell carcinoma; Adenocarcinoma; X-ray computed tomography; Radiomics

Core Tip: In this study, multiscale and multiphase computed tomography (CT)-based radiomics models were constructed and evaluated to discriminate squamous cell carcinoma and adenocarcinoma of the esophagogastric junction (CEGJ) before operation. The results demonstrated that the combination of multiphase 3D CT radiomics features could improve the differentiation performance than 2D CT radiomics or single-phase-based radiomics. Therefore, radiomics method could help open up a new field for noninvasive diagnosis and personalized management of CEGJ.

Citation: Du KP, Huang WP, Liu SY, Chen YJ, Li LM, Liu XN, Han YJ, Zhou Y, Liu CC, Gao JB. Application of computed tomography-based radiomics in differential diagnosis of adenocarcinoma and squamous cell carcinoma at the esophagogastric junction. *World J Gastroenterol* 2022; 28(31): 4363-4375
URL: https://www.wjgnet.com/1007-9327/full/v28/i31/4363.htm
DOI: https://dx.doi.org/10.3748/wjg.v28.i31.4363

INTRODUCTION

Carcinoma of the esophagogastric junction (CEGJ) is defined as a carcinoma whose center is located within 5 cm above and below the esophagogastric anatomical junction and crosses the esophagogastric junction (EGJ). Due to the short and narrow EGJ site and the up-and-down invasive nature of the CEGJ, its biological behavior is different from that of gastric or esophageal cancer[1-3]. The Siewert staging, which is widely accepted in academia, classifies CEGJ into types I, II, and III based on the distance between the tumor center and the EGJ[4]. Because of the infiltrative growth pattern of the tumor, the distance between the tumor center and the EGJ in CEGJ is difficult to measure accurately, and Siewert staging is often not easy to determine directly. Squamous cell carcinoma of the esophagogastric junction (SCCEG) has different clinicopathological features from adenocarcinoma of the esophagogastric junction (AEG). Based on the results from previous research, mediastinal lymph node metastases are more likely to occur in SCCEG above the EGJ, whereas metastases from the AEG under the EGJ probably appear in the abdomen[5,6]. Differentiating SCCEG from AEG can indicate Siewert stage and whether the surgical route for patients with CEGJ is transthoracic or transabdominal, as well as aid in determining the extent of lymph node dissection. With the development of neoadjuvant therapy,

preoperative determination of pathological type can help in the selection of neoadjuvant radiotherapy and chemotherapy regimens.

Clinically, medical imaging plays a supporting role in pathological classification and tumor staging. Conventional computed tomography (CT), magnetic resonance imaging, and positron emission tomography rely primarily on the visual assessment of the imaging physician and have limitations in early identification of the pathological type of CEGJ. Although histological biopsies are commonly used in clinical practice, some patients have contraindications or low tolerance, and the biopsy sample is limited to the mucosal surface, which may provide an inadequate assessment of the entire tumor status [7]. Therefore, it is important to explore a reliable, practical, and non-invasive preoperative histological staging method for CEGJ, which is clinically important for neoadjuvant radiotherapy, surgical approach selection, and lymph node dissection in CEGJ patients. Radiomics technique uses a combined medical-industrial approach to transform traditional images into digital quantitative features, which has potential for digging the potential biological characteristics and heterogeneity of tumor images and has been widely and non-invasively used in the diagnosis, differential diagnosis, and disease evaluation[8-12]. Radiomics technique has also been studied in the differential diagnosis of squamous lung cancer and adenocarcinoma[13,14]. However, it is still unclear whether radiomics features extracted from CT images would be useful in predicting pathological type in patients with CEGJ.

Both of two-dimensional (2D) cross section or three-dimensional (3D) volume in CT images could be delineated for radiomics feature extraction. The reported radiomics-based gastric cancer studies have either utilized 2D or 3D segmentation[12,15]. However, it remains unclear whether to apply 2D or 3D regions of interest (ROIs) for pathological typing. The selection of 2D or 3D ROIs for outlining can influence radiomics feature values, feature stability, feature screening, and discriminative model performance[16-18]. And the controversy still exists for the performance of diagnosis or prognosis between 2D and 3D radiomics in tumor[16-18].

Therefore, in the current study, we aimed to construct and evaluate the multiscale and multiphase CT-based radiomics to discriminate SCCEG and AEG. The developed CT-based models might provide assistance in the personalized and precise treatment of clinical CEGJ patients, especially in the selection of surgical approach and determination of the extent of lymph node dissection.

MATERIALS AND METHODS

Patient selection

With institutional review board approval (ethical approval number: 2021-ky-1070-002) and waiver of the written informed consent, we retrospectively collected patients with SCCEG confirmed by gastroscopy and surgical pathology at the First Affiliated Hospital of Zhengzhou University from January 2010 to June 2021. The patient enrollment criteria included: (1) CT-enhanced abdominal examination within 30 d before surgery; (2) Complete clinicopathological data available; (3) The lesion covers at least 3 slices on CT cross section, and the maximum plane diameter is not less than 2 cm; and (4) No neoadjuvant chemoradiotherapy prior to CT examination. The exclusion criteria included: (1) Patient's history of other malignant tumors in combination; (2) Poor CT image quality or lack of raw DICOM data; and (3) Combined heart, lung, and other important organ dysfunction which could not allow CT examination to be performed. Finally, 130 patients with SCCEG were included, including 87 males and 43 females, aged 38-89 (65.72 ± 8.84) years, with a disease duration of 5 d to 4 years and main symptoms of dysphagia, obstructive sensation of eating, and abdominal pain. Another 130 patients with AEG who were matched with the SCCEG patients were also recruited, including 93 males and 37 females, aged 31-83 (62.95 ± 9.91) years.

CT image acquisition

Informed consent forms were signed before all patients underwent contrast-enhanced CT scans. CT scans were acquired using a 64-row CT scanner (GE Healthcare, Discovery CT 750 HD, United States) or 256-row CT scanner (GE Healthcare, Revolution CT, United States). Preparation for the examination: fasting for more than 8 h before the examination, intramuscular injection of scopolamine 10-20 mg 15-20 min before the examination to reduce gastrointestinal motility (Hangzhou Minsheng Pharmaceutical PG Roup Co., Ltd. Specifications: 10 mg/mL), and perform breath-holding exercises. Drink 800-1 000 mL of warm water 10 to 15 min before the examination. Scanning parameters: tube voltage 120 kV, tube current using automatic milliampere second technology, pitch 1.375/1.1; field of view (FOV) of 500 mm; 512 mm x 512 mm matrix, scan thickness 0.625mm to 5 mm, scan spacing 0.625mm to 5mm. Scan area: at least encompasses the lower esophagus to the lower border of both kidneys. Enhancement scan: 90-100 mL of non-ionic contrast agent was injected through the elbow vein using a high-pressure syringe (GE Medical Systems, iopromide, 370 mg/mL).

Image processing and segmentation

The arterial- and venous-phase CT images were isotropically resampled with a voxel size of 1 mm × 1 mm × 1 mm by using the trilinear interpolation in the Artificial Intelligence Kit software (A.K, version:

3.3.0.R, GE Healthcare, United States), in order to minimize the effect of different scanning protocols or equipment on quantitative inhomogeneity of histological features[19]. 2D ROIs were outlined along the largest cross-sectional area in the axial plane of CT images. After delineating the tumor cross-sectional area slice-by- slice in the axial plane, 3D ROIs were finally merged into volume of interest (VOI) (Figures 1 and 2). Care should be taken to avoid the gastric cavity and stomach contents, fatty tissue around the stomach wall, and blood vessels when segmenting. The 2D ROI or 3D VOI delineation was conducted by a radiologist (Chen YJ, 6 years of experience in imaging diagnosis). In order to ensure the reliability and reproducibility of the radiomics features, 30 patients were randomly selected to be segmented in a 2D and 3D manner. For inter-observer agreement analysis, when the radiologist (Chen YJ) conducted the first-time whole-dataset segmentation, another radiologist (Huang WP, 7 years of experience in imaging diagnosis) delineated the selected 30 patients at the same period. For intra-observer agreement analysis, the radiologist (Chen YJ) repeatedly conducted the segmentation 1 mo after the first-time delineation.

Radiomics feature extraction

The 2D or 3D radiomics features were extracted with open-source Python package Pyradiomics[20]. There were respectively 1409 radiomics features extracted from 2D or 3D ROIs in the arterial or venous phase. The original images and the transformed images based on different filters were mainly used for feature extraction. A total of 107 features were extracted from the original images, including 18 intensity statistical and 14 shape-based features. There were 75 textural features extracted from Gray Level Cooccurrence Matrix (GLCM), Gray Level Run Length Matrix (GLRLM), Gray Level Size Zone Matrix (GLSZM), Gray Level Dependence Matrix (GLDM), and Neighboring Gray Tone Difference Matrix (NGTDM). In addition, the same number of first-order grayscale statistical features and texture features were extracted based on different transformed images. A total of 744 features were extracted based on wavelet decomposition images with eight filter channels, 279 features were extracted based on Laplacian of Gaussian (LoG) transform images (sigma parameters selected as 1.0 mm, 3.0 mm, and 5.0 mm), and 279 features were extracted based on Local Binary Pattern (LBP) filtered images (2^{nd} order spherical harmonic function, spherical neighborhood operator with radius 1.0 and fine fraction 1)[20]. The features were extracted by discretizing the CT values within the ROIs based on a fixed interval width (bin width = 25 HU). The 2D and 3D radiomics features extracted from the randomly selected patients were used to calculate the intra-/inter-class correlation coefficients (ICCs). 2D or 3D features with intra- and inter-observer ICC values simultaneously greater than 0.75 were retained, which meant that the features with good repeatability were involved in the further analysis[18,21].

Feature selection and model construction

The 260 cases of data were divided into a training group and an internal test group by randomly stratified sampling at a ratio of 7:3. The training group was mainly used for preprocessing parameter determination, and feature screening and modeling, and the same treatment process, parameters, and model were applied to the test group for internal test. The same method was used for feature preprocessing and feature screening in the arterial and venous phase training samples, and independent arterial and venous radiomics models were established. The feature selection and final modeling procedure were performed as follows. The features were first preprocessed by excluding features with variance < 1.0, filling missing values with the median and *Z*-score normalization, and excluding collinear features with a cut-off value of correlation coefficients larger than 0.7. Then the Mann-Whitney *U*-test or *t*-test was used to select features with a significant difference between two classes ($P < 0.05$). The least absolute shrinkage and selection operator (LASSO) logistic regression (minimum binomial deviance) with 10-fold cross validation was conducted to avoid overfitting and the features with non-zero coefficients were retained[22]. Finally, the retained features were inputted into backward stepwise logistic regression with the minimum Akaike Information Criterion (AIC) to develop the regression radiomics model. The "Radscore" of each patient was calculated according to the formula (Radscore = $\beta_0 + \sum\beta_i x_i$, β_0 is a constant term and βi is the regression coefficient of the feature *x*i).

Four independent radiomics models were constructed, including: 2D arterial-phase model ($Radscore^{AP\_2D}$), 2D venous-phase model ($Radscore^{VP\_2D}$), 3D arterial-phase model ($Radscore^{AP\_3D}$), and 3D venous-phase model ($Radscore^{VP\_3D}$). Two combined models were derived based on the established independent model Radscore according to the regression formula (Radscore = $\beta_0 + \sum\beta_i x_i$, β_0 is a constant term and βi is the logistic regression coefficient of the model score *x*i). And the 2D arterial-venous combined model 3 ($Radscore^{AP\_VP\_2D}$) and 3D arterial-venous combined model ($Radscore^{AP\_VP\_3D}$) were established.

Evaluation of model predictive performance

The performance of the models was evaluated by using receiver operating characteristic curve (ROC) analysis to obtain the area under the ROC curve (AUC). The sensitivity, accuracy, negative predictive value, and positive predictive value were calculated based on the cut-off values corresponding to the maximum Youden index to evaluate the discrimination performance of the models. The cut-off values of the training group were applied to the test group to obtain their corresponding ROC parameters in

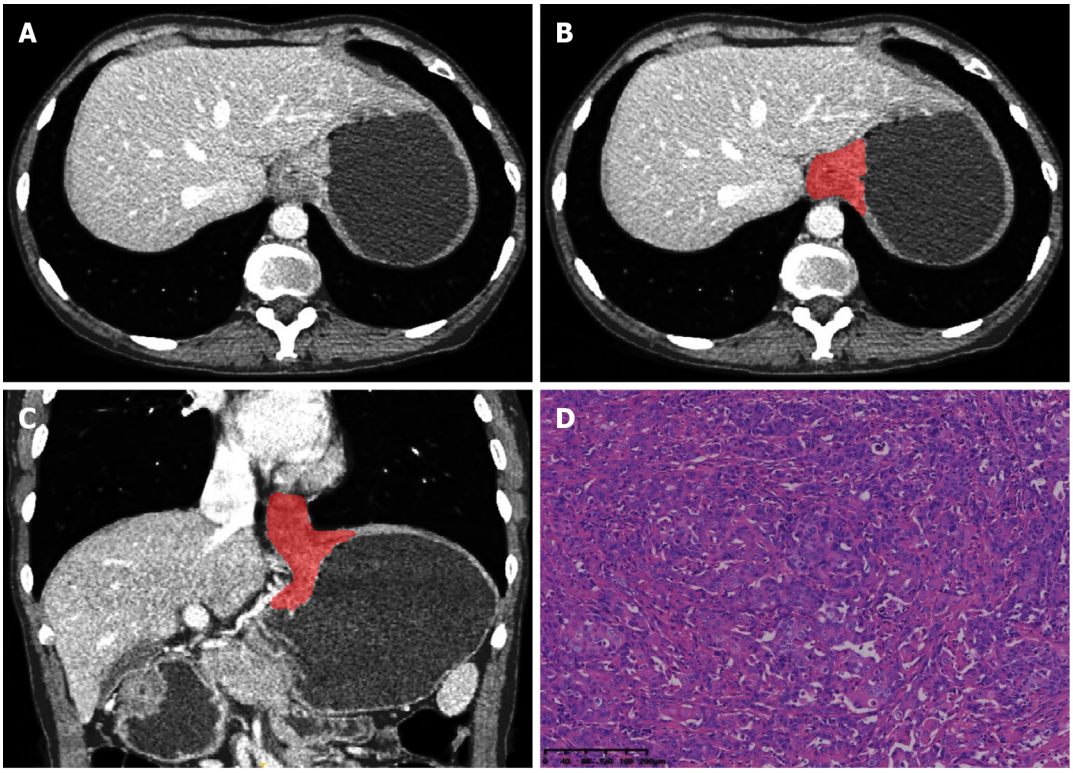

DOI: 10.3748/wjg.v28.i31.4363 **Copyright** ©The Author(s) 2022.

Figure 1 A 43-year-old man with squamous cell carcinoma of the esophagogastric junction. A: Axial computed tomography image in venous phase; B: Schematic diagram of 2D region of interest (ROI) segmentation on ITK-SNAP software; C: Schematic diagram of 3D ROI segmentation on ITK-SNAP software; D: Postoperative pathological image confirming squamous cell carcinoma of the esophagogastric junction (HE staining, × 200).

the test group. The calibration curve analysis and the Hosmer-Lemeshow test were used for evaluating model calibration and the goodness of fit ($P > 0.05$ indicates a good model fit). Delong's test was used to compare the AUC between paired models. Continuous net reclassification improvement (NRI) and integrated discrimination improvement (IDI) were used to assess ability of the models in improving the classification effectiveness[18]. The decision curve analysis (DCA) was used to assess the net clinical benefit or clinical utility of each model at different threshold probabilities.

Statistical analysis

R software (version 3.6.3, http://www.r-project.org) was applied for statistical analyses in the current study. Radiomics features and Radscore are continuous variables, and data normality was tested using kurtosis and skewness values, and comparisons between two groups were made using independent samples *t*-test (for data with a normal distribution) or Mann-Whitney *U* test (for data not following a normal distribution). Categorical variables were tested by chi-square test or Fisher's exact test. A two-sided $P < 0.05$ was considered statistically significant. The optimism of the prediction accuracy of the model was validated using 1000-times Bootstrap in the training group. The following R packages were applied: "icc" for intra-/inter-class correlation coefficient; "glmnet" for logistic regression; "pROC" for ROC analysis; "rmda" for DCA; calibration function in the "rms" package for calibration analysis, and the "PredictABEL" package for NRI and IDI analysis.

RESULTS

Feature screening and model construction

Arterial phase model based on 2D ROI: A total of 175 radiomics features (ICCs > 0.75) were retained among 1409 features. There were 61 and 6 features retained rafter variance and correlation analysis, respectively. Among 6 features screened by univariate analysis and 10-fold cross validation LASSO regression (Figure 3A and B), 5 were further selected by stepwise logistic regression analysis. The Radscore^{AP_2D} is summarized in Supplementary Figure 1. The results of ICCs for individual features are shown in Supplementary Table 1 and the multivariable logistic regression results of features involved in the model are summarized in Supplementary Table 2. ROC curves for single 2D arterial features to identify SCCEG and AEG are shown in Supplementary Figure 2A and The 2D arterial model radiomics

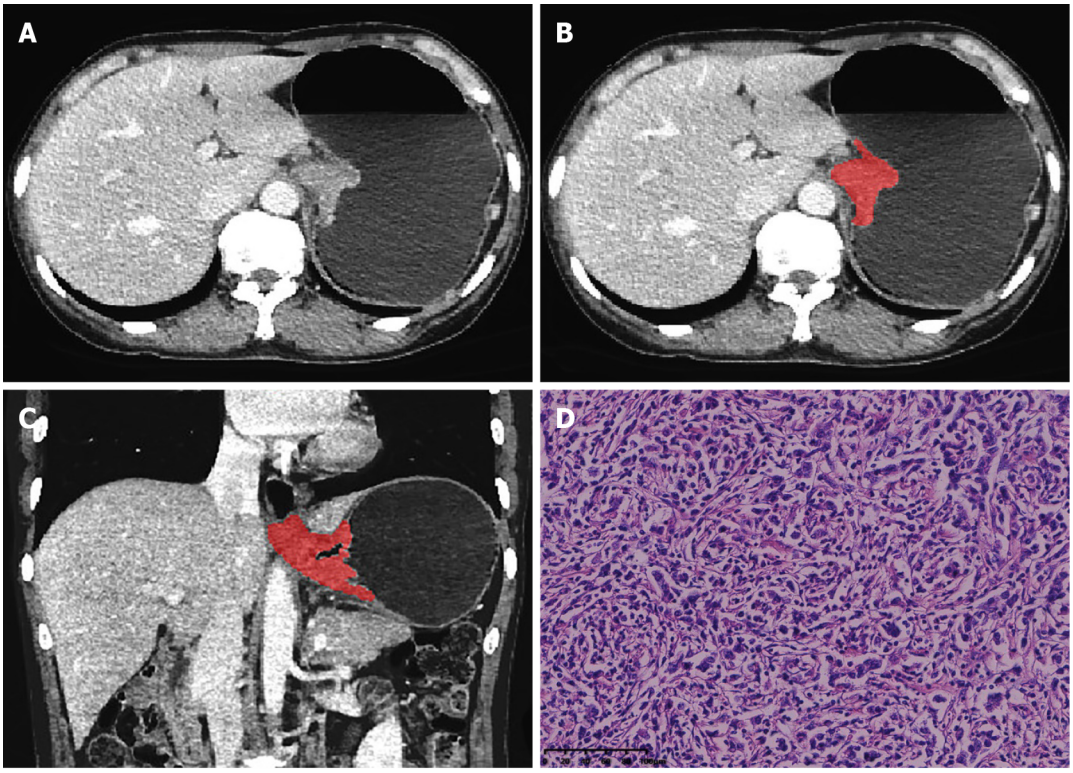

DOI: 10.3748/wjg.v28.i31.4363 **Copyright** ©The Author(s) 2022.

Figure 2 A 56-year-old man with adenocarcinoma of the esophagogastric junction. A: Axial computed tomography image in venous phase; B: Schematic diagram of 2D region of interest (ROI) segmentation on ITK-SNAP software; C: Schematic diagram of 3D ROI segmentation on ITK-SNAP software; D: Postoperative pathological image confirming adenocarcinoma of the esophagogastric junction (HE staining, × 200).

features and the differences of Rad-score^{AP_2D} in the training and test groups are shown in Supplementary Table 3.

Venous phase model based on 2D ROI: A total of 275 radiomics features (ICCs > 0.75) were retained among 1409 features. There were 124 and 12 features kept after variance and correlation analysis, respectively. Among 6 features screened by univariate analysis and 10-fold cross validation LASSO regression (Figure 3C and D), 5 were kept by stepwise logistic regression analysis. The Radscore^{VP_2D} is summarized in Supplementary Figure 3. The results of ICCs for individual features are shown in Supplementary Table 4 and the multivariable logistic regression results of features involved in the model are summarized in Supplementary Table 5. ROC curves for single 2D venous features to identify SCCEG and AEG are illustrated in Supplementary Figure 2C and The 2D venous model radiomics features and the differences of Rad-score^{VP_2D} in the training and test groups are shown in Supplementary Table 6.

Arterial phase model based on 3D ROI: A total of 714 radiomics features (ICCs > 0.75) were retained among 1409 features. There were 358 and 27 features kept after variance and correlation analysis, respectively. Among 15 features screened by univariate analysis and 10-fold cross validation LASSO regression (Figure 3E and F), 10 were kept by stepwise logistic regression analysis. The Radscore^{AP_3D} is summarized in Supplementary Figure 4. The ICCs for individual features are shown in Supplementary Table 7 and the multivariable logistic regression results of features involved in the model are summarized in Supplementary Table 8. ROC curves for single 3D arterial features to identify SCCEG and AEG are shown in Supplementary Figure 2E and the 3D arterial model radiomics features and the differences of Rad-score^{AP_3D} in the training and test groups are summarized in Supple-mentary Table 9.

Venous phase model based on 3D ROI: A total of 774 radiomics features (ICCs>0.75) were retained among 1409 features. There were 355 and 23 features kept after variance and correlation analysis, respectively. Among 8 features screened by univariate analysis and 10-fold cross validation LASSO regression (Figure 3G and H), 7 were kept by stepwise logistic regression analysis, and the Radscore^{VP_3D} is summarized in Supplementary Figure 5. The ICCs result for individual features are shown in Supplementary Table 10 and the multivariable logistic regression results of features involved in the model are summarized in Supplementary Table 11. ROC curves for single 3D venous features to identify SCCEG and AEG are shown in Supplementary Figure 2G and The 3D venous model radiomics features and the differences of Rad-score^{VP_3D} in the training and test groups are summarized in

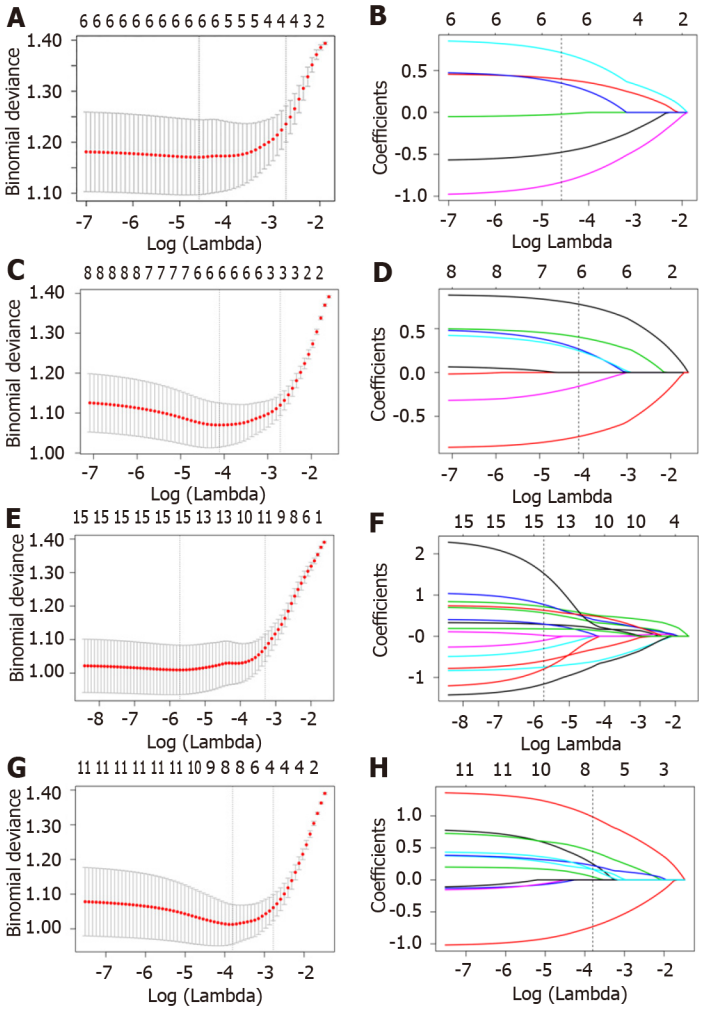

DOI: 10.3748/wjg.v28.i31.4363 **Copyright** ©The Author(s) 2022.

Figure 3 Least absolute shrinkage and selection operator logistic regression feature screening graphs. The radiomics feature screening using the least absolute shrinkage and selection operator regression was performed to select the optimal model parameter λ using 10-fold cross-validation. A, C, E, and G: Graphs of binomial deviation of 2D-arterial model, 2D-venous model, 3D-arterial model, and 3D-venous model with parameter λ, respectively. The dashed lines indicate the selected optimal log(λ) values and the location of one standard error; B, D, F, and H: Graphs of variation of the radiomics characteristic coefficients with log(λ) for 2D-arterial model, 2D-venous model, 3D-arterial model, and 3D-venous model, respectively. The dotted line indicates the location of the selected optimal log(λ) value.

Supplementary Table 12.

2D arterial-venous combined model

By combining Radscore^{AP_2D} and Radscore^{VP_2D}, the 2D arterial-venous combined model was derived and the Radscor^{AP_VP_2D} is described in Supplementary Figure 6.

3D arterial-venous combined model

By combining Radscore^{AP_3D} and Radscore^{VP_3D}, the 3D arterial-venous combined model was derived and the Radscor^{AP_VP_3D} is summarized in Supplementary Figure 7.

In this study, a total of 10 candidate radiomics feature parameters were screened out in 2D arterial and venous phase images, mostly first-order features and texture features extracted based on Log transformed or wavelet transformed images, and the main categories included 4 first-order features, 2 GLRLM features, 2 GLSZM features, 1 GLDM feature, and 1 NGTDM feature. More features were screened out in the 3D arterial phase and venous phase images—17 in total, and the main categories included 6 first-order features, 4 GLDM features, 4 NGTDM features, 1 GLRLM feature, 1 GLSZM feature, and 1 GLCM feature.

Radiomics model performance

The AUC, specificity, sensitivity, accuracy, positive predictive value, and negative predictive value of the 6 models developed in this study to discriminate SCCEG from AEG in the training and test groups

are summarized in Table 1, and the ROC curves are shown in Figure 4. The model optimism was assessed by 1000-times bootstrap as shown in Table 2. It indicated that the 2D-arterial, 2D-venous, 3D-arterial, and 3D-venous model presented a degree of optimism less than 0.1 during repeated sampling. The Delong test results in the training and test groups are shown in Supplementary Table 13. All the 2D models had an AUC greater than 0.800 in the test group, except for the arterial model, which had an AUC of 0.752 in the test group. The AUC values of the venous model were higher than those of the arterial model (0.849 *vs* 0.808 and 0.831 *vs* 0.752) in both the training and test groups. All the 3D models had a higher AUC in the venous model than in the arterial model. In the combined models, both the 3D and 2D models were higher than their independent phase model both in the training and test groups. When comparing the performance between 2D and 3D models, the results showed that no matter for the independent phase model or the multi-phase-combined model, 3D models performed with a higher AUC than 2D models. Among all the models, the 3D-arterial-venous combined model had the highest AUC values of 0.904 and 0.901 in the training and test groups, respectively. As some statistical significance was not obvious during the Delong test, continuous NRI and IDI analyses were performed to evaluate the ability of each model for improving the classification and the results are shown in Supplementary Table 14. In both the training and test groups, the venous model demonstrated a positive improvement in discrimination over the arterial model (NRI > 0, IDI > 0), the 3D-venous model demonstrated a significant positive improvement in discrimination over the 2D-venous model (P < 0.05), both in the 3D model and in the 2D model, the combined model demonstrated a significant positive improvement in discrimination over the arterial model (P < 0.05); the 3D combined model reflected a significant positive improvement in discrimination compared with the 2D combined model (P < 0.05). In addition, the calibration curve (Figure 5) and the results of the Hosmer-Lemeshow test (Supplementary Table 15) indicate that the six models had good calibration. The clinical utility of the model was confirmed by the decision curve (Figure 6), in which the 3D-arterial-venous combined model and the 3D-venous model had higher net benefits in the test group within a threshold probability interval of 0.3-1.

DISCUSSION

In the current study, the multiscale and multiphase CT-based radiomics method was used to preoperatively discriminate SCCEG and AEG. The results showed that the combination of multiphase 3D CT radiomics features could improve the differentiation performance. Therefore, radiomics method could help open up a new field for noninvasive diagnosis and personalized management of CEGJ. Histopathology biopsy is a commonly used clinical method, and these radiomics features are considered to be complementary to histology biopsy but not a complete substitute for histopathology at this time. Repeat biopsy or endoscopic ultrasound deeper biopsies should be recommended if upper endoscopic biopsies are inconclusive or if it conflicts with the results suggested by radiomics features. Radiomics can provide an adequate reference if the patient has contraindications and low tolerance to endoscopic biopsy.

Previous studies have focused on the quantitative parameters of spectral CT. Zhou *et al*[23] found that the normalized iodine concentration, the $K_{40\text{-}70\ keV}$, and the effective atomic number in the arterial phase could identify SCCEG and AEG; the AUC values were 0.720, 0.730, and 0.706, respectively. Radiomics uses mathematically describable imaging features to comprehensively analyze tumor heterogeneity[24], and has not been validated for identifying SCCEG from AEG. Therefore, we tried to use radiomics features to identify the pathological type of CEGJ by comprehensively considering the effectiveness of different phases and segmentation method. In this study, more features were screened out in the 3D models of different phases than in the 2D models, which is related to the fact that the 3D ROIs contain the lesion as a whole and the extracted features have a larger distribution. The results showed that the efficacy of the venous features was higher than that of the arterial features in identifying SCCEG from AEG. Pathologically, squamous carcinoma grows faster and tends to grow in a swelling superposition with denser tissue structure, while adenocarcinoma mostly grows in an appendicular pattern with looser tissue structure[25]. With the prolongation of scanning time, the contrast agent continuously penetrates into the interstitial space of tumor cells, and more textural features appear in the venous phase, which better reflects the heterogeneous characteristics of squamous carcinoma. Tumor vascularization is a kind of biological behavior that reconstructs nutrition connection and promotes tumor development. Pathologic types, tumor origin, and structure of the microvasculature affect the enhancement pattern and radiomics-based parameters.

We found that among the features retained in the venous model, Dependence variance (GLDM) and Large dependence high gray level emphasis (GLDM) had larger weight in the 3D and 2D models, respectively. GLDM mainly describes the degree of dependence between voxel gray levels, and the SCCEG group reflects the high "Dependence variance" of 3D gray levels and the "Large dependence high gray level emphasis" of 2D gray levels, which reflects the large gray level heterogeneity of squamous cancer tissue in 3D features and the high gray level distribution in 2D features from texture features. The uneven distribution of tumor vessels in squamous carcinoma lesions is prone to tumor cell

Table 1 Model performance for differentiating squamous cell carcinoma of the esophagogastric junction and adenocarcinoma of the esophagogastric junction in the training and validation groups

	2D-ROI models			3D-ROI models		
Model	**Artery**	**Venous**	**Artery + venous**	**Artery**	**Venous**	**Artery + venous**
Training group						
AUC	0.808	0.849	0.869	0.876	0.877	0.904
95%CI	0.744-0.872	0.792-0.905	0.818-0.920	0.827-0.926	0.827-0.927	0.861-0.947
Threshold	0.095	-0.101	-0.370	-0.149	-0.352	0.043
Specificity	0.802	0.758	0.681	0.813	0.780	0.879
Sensitivity	0.736	0.802	0.890	0.824	0.857	0.802
Accuracy	0.769	0.780	0.786	0.819	0.819	0.841
NPV	0.753	0.793	0.861	0.822	0.845	0.816
PPV	0.788	0.768	0.736	0.815	0.796	0.869
Validation group						
AUC	0.752	0.831	0.845	0.824	0.879	0.901
95%CI	0.640-0.864	0.742-0.921	0.763-0.928	0.732-0.917	0.798-0.960	0.830-0.973
Threshold	0.095	-0.101	-0.370	-0.149	-0.352	0.043
Specificity	0.795	0.692	0.718	0.769	0.667	0.821
Sensitivity	0.641	0.769	0.769	0.744	0.872	0.795
Accuracy	0.718	0.731	0.744	0.756	0.769	0.808
NPV	0.689	0.750	0.757	0.750	0.839	0.800
PPV	0.758	0.714	0.732	0.763	0.723	0.816

ROI: Region of interest; AUC: Area under the curve; NPV: Negative predictive value; PPV: Positive predictive value.

Table 2 Model optimism estimation by 1000-times bootstrap in the training group

Index	Model	Apparent AUC[1]	AUC Bootstrap-test[2] (mean, 95%CI)	Optimism
1	2D-arterial model	0.808	0.770 (0.767-0.772)	0.050
2	2D-venous model	0.849	0.820 (0.817-0.822)	0.036
3	3D-arterial model	0.876	0.815 (0.812-0.880)	0.080
4	3D-venous model	0.877	0.833 (0.830-0.835)	0.056

[1]The area under the curve of predictive model developed in the whole training dataset.
[2]The averaged model performance in the "out-of-bag" test set after 1000-times bootstrap. AUC: Area under the curve.

degeneration and necrosis, and it is speculated that the grayscale distribution of squamous carcinoma lesions has some complexity in different transformed images. In addition, features prevalent in the arterial and venous models are Busyness (NGTDM), Dependence variance (GLDM), first order grayscale features. NGTDM features can also represent a certain degree of grayscale distribution inhomogeneity. NGTDM describes the difference between adjacent grayscale values and average grayscale values within the quantized distance of the adjacent grayscale difference matrix, and the squamous carcinoma exhibits a high "Busyness", representing rapid intensity changes between pixels and their neighbors and reflecting the heterogeneous nature of the tissue. In addition, the first-order statistical gray value features calculated based on different dimensions and different phases of images were selected into each model simultaneously, indicating that the images of the SCCEG group in different phases and dimensions have lower gray values, which may be attributed to the histopathological inhomogeneity of microvessels within squamous carcinoma, less blood supply than adenocarcinoma, and lower gray statistical values in squamous carcinoma than adenocarcinoma.

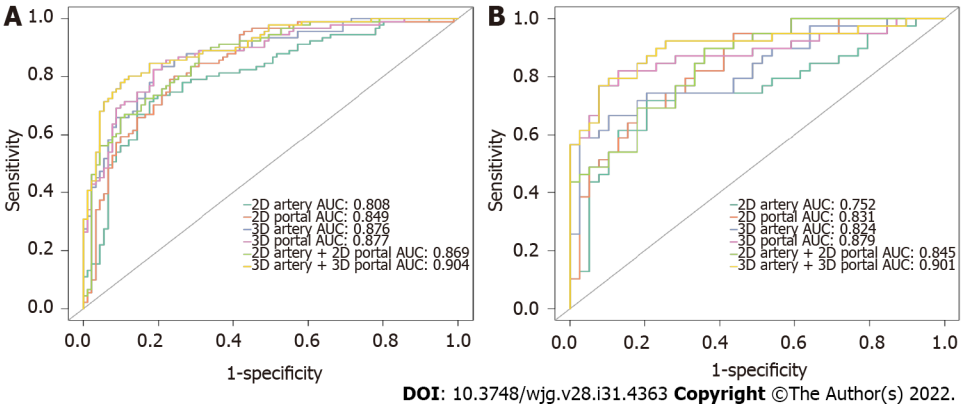

DOI: 10.3748/wjg.v28.i31.4363 **Copyright** ©The Author(s) 2022.

Figure 4 Receiver operating characteristic curves of different models to identify squamous cell carcinoma and adenocarcinoma of the esophagogastric junction. A: Training group; B: Test group.

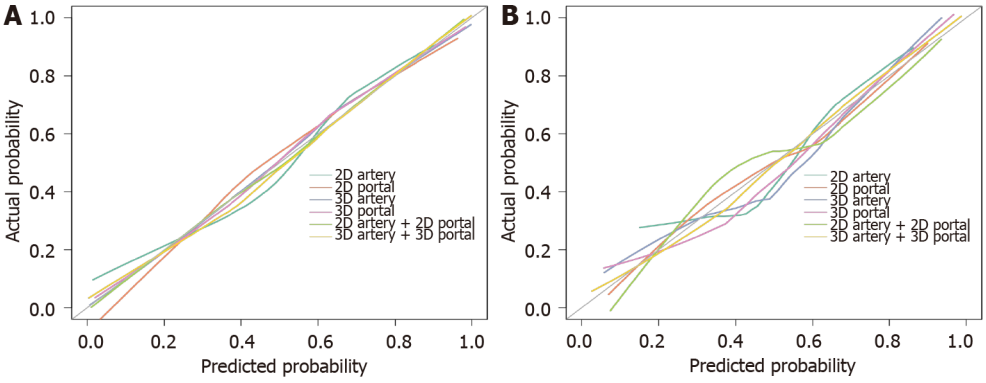

DOI: 10.3748/wjg.v28.i31.4363 **Copyright** ©The Author(s) 2022.

Figure 5 Calibration curves of 2D-arterial model, 2D-venous model, 3D-arterial model, 3D-venous model, 2D arterial-venous combined model, and 3D arterial-venous combined model to identify squamous cell carcinoma of the esophagogastric junction and adenocarcinoma of the esophagogastric junction. A: Training group; B: Test group.

For both of 2D and 3D models, the AUC difference was statistically significant between the arterial-venous combined model and the independent arterial model, while not significant between the arterial-venous combined model and the independent venous model. It suggested that the venous phase might contribute more predictive information compared with the arterial phase. Combining the NRI and IDI index results, the venous model showed a positive improvement in discrimination compared to the arterial model, and the 3D model showed a significant positive improvement in discrimination compared to the 2D model as well.

Most previous radiomics studies varied in the utilization of 2D or 3D segmentation. However, different delineation methods may result in different feature values and predictive performance. The study of different dimensional outlining approaches and the corresponding model performance can guide radiomics practice in related disease areas. Zhao *et al*[15] developed a dual-energy CT–based nomogram for noninvasive identification of the status of HER2 expression in gastric cancer, and both 2D and 3D radiomics nomograms performed well. Huang *et al*[18] found that the efficacy of the 3D model was superior to the 2D model when they developed 2D and 3D radiomics models to predict the aggressiveness of pancreatic solid pseudopapillary tumors. This study showed that in the discrimination of SCCEG and AEG, the use of 3D radiomics-based on CT images will be beneficial to improve the discrimination, but the time required for 3D segmentation was significantly longer than that of 2D, so it is also necessary to consider the improvement and optimization of automatic 3D lesion segmentation.

This study still has some limitations. First, the lesion morphology of CEGJ is not fixed, and manual segmentation methods are required. While the lesion travels along the gastric and esophageal walls in a tortuous manner, the consistency and stability of the annotation will affect the efficacy of the model. In this study, features with ICCs > 0.75 were used for subsequent analysis, which ensured the robustness of the radiomics features to some extent. More candidate semi-automatic or automatic segmentation algorithms would be welcomed to improve clinical efficiency. Second, our study was previously reported to include data on squamous cell carcinoma of the cardia or distal esophagus, but it is still a single-center retrospective study with a small sample size, especially for SCCEG, which inevitably

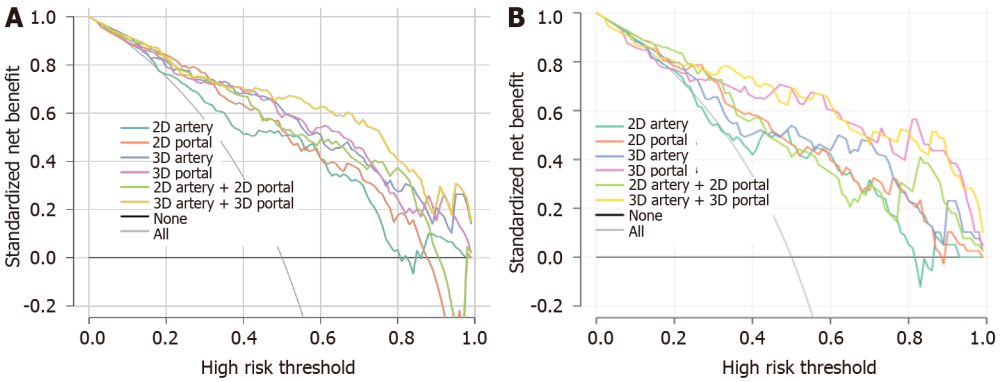

DOI: 10.3748/wjg.v28.i31.4363 **Copyright** ©The Author(s) 2022.

Figure 6 Decision curves for 2D-arterial model, 2D venous model, 3D-arterial model, 3D venous model, 2D arterial-venous combined model, and 3D arterial-venous combined model. A: Training group; B: Test group. The black horizontal line indicates no lesions as squamous cell carcinoma (NONE) and the grey line indicates all lesions as squamous cell carcinoma (ALL). The colored lines of each model respectively illustrate the net benefit brought to each patient. The closer the decision curves to the black and gray curves, the similar the clinical decision net benefit of the model compared with "treat ALL" or "treat NONE" decision. When comparing different models, the higher the model curve within the same threshold probability, the higher the clinical net benefit resulting from the model.

generates selectivity bias when paired with a larger number of AEGs. Future multicenter, prospective, large sample studies are needed to further improve and validate the diagnostic efficacy and generalization ability of the model. In addition, the main purpose of the current study was to evaluate the usefulness of 2D- or 3D-based radiomics methods and clinical data or laboratory test indicators were not included. There is much room for improvement of model reliability, which will be further collected in future studies in order to obtain a more comprehensive understanding.

CONCLUSION

In conclusion, multi-scale and multi-phase radiomics models based on CT imaging data were developed and validated for differentiating SCCEG from AEG before the operation in our study. The 3D radiomics model combining arterial and venous phase images showed encouraging performance than the corresponding 2D model. These models require further validation as decision support tools to guide clinical practice and develop individualized treatment plans for CEGJ patients. Currently, histopathological biopsy is still the common method of diagnosis.

ARTICLE HIGHLIGHTS

Research background

Differentiating squamous cell carcinoma of the esophagogastric junction (SCCEG) from adenocarcinoma of the esophagogastric junction (AEG) can indicate Siewert stage and whether the surgical route for patients with carcinoma of the esophagogastric junction (CEGJ) is transthoracic or transabdominal, as well as aid in determining the extent of lymph node dissection. With the development of neoadjuvant therapy, preoperative determination of pathological type can help in the selection of neoadjuvant radiotherapy and chemotherapy regimens.

Research motivation

Radiomics technique uses a combined medical-industrial approach to transform traditional images into digital quantitative features, which has potential for digging the potential biological characteristics and heterogeneity of tumor images and has been widely and non-invasively used in the diagnosis, differential diagnosis, and disease evaluation. However, to the best of our knowledge, there is no literature that has evaluated whether a radiomics signature derived from computed tomography (CT) images would be useful in predicting pathological type in patients with CEGJ.

Research objectives

In the current study, we proposed a CT radiomics-based classification method by considering the performance of 3D or 2D segmentation and multiple CT imaging phases to discriminate SCCEG and AEG.

Research methods

We retrospectively analyzed the preoperative contrasted-enhanced CT imaging data of single-center patients with pathologically confirmed SCCEG (n = 130) and AEG (n = 130). One thousand four hundred and nine radiomics features were separately extracted from 2D or 3D regions of interest in arterial and venous phases. Totally, 6 logistic regression models were established based on 2D and 3D multi-phase features.

Research results

The venous model showed a positive improvement compared with the arterial model (NRI > 0, IDI > 0), and the 3D-venous and combined models showed a significant positive improvement compared with the 2D-venous and combined models (P < 0.05). Decision curve analysis showed that the combined 3D-arterial-venous model and 3D-venous model had a higher net clinical benefit within the same threshold probability range in the test group.

Research conclusions

The combined arterial-venous CT radiomics model based on 3D segmentation can improve the performance in differentiating EGJ squamous cell carcinoma from adenocarcinoma.

Research perspectives

These models require further validation as decision support tools to guide clinical practice and develop individualized treatment plans for CEGJ patients.

FOOTNOTES

Author contributions: Du KP and Huang WP designed the research; Liu SY and Li LM performed the research; Chen YJ, Han YJ, Zhou Y, and Liu CC collected the data; Du KP and Huang WP analyzed the data and wrote the paper; Gao JB reviewed the paper; and all authors have read and approved the final manuscript.

Institutional review board statement: The study was approved by the Institutional Review Board at the First Affiliated Hospital of Zhengzhou University (No. 2021-ky-1070-002).

Conflict-of-interest statement: The authors declare that they have no competing interests to disclose.

Data sharing statement: All data generated or analyzed during this study are included in this published article.

Country/Territory of origin: China

ORCID number: Ke-Pu Du 0000-0002-3870-7656; Wen-Peng Huang 0000-0002-9104-1494; Si-Yun Liu 0000-0001-5611-382X; Yun-Jin Chen 0000-0002-2147-0912; Li-Ming Li 0000-0002-2910-9742; Yi-Jing Han 0000-0001-7358-0139; Yue Zhou 0000-0001-7781-7228; Chen-Chen Liu 0000-0001-5026-3288; Jian-Bo Gao 0000-0003-2621-3701.

S-Editor: Ma YJ
L-Editor: Wang TQ
P-Editor: Ma YJ

REFERENCES

1 **Sun X**, Wang G, Liu C, Xiong R, Wu H, Xie M, Xu S. Comparison of short-term outcomes following minimally invasive versus open Sweet esophagectomy for Siewert type II adenocarcinoma of the esophagogastric junction. *Thorac Cancer* 2020; **11**: 1487-1494 [PMID: 32239662 DOI: 10.1111/1759-7714.13415]
2 **Wang T**, Wu Y, Zhou H, Wu C, Zhang X, Chen Y, Zhao D. Development and validation of a novel competing risk model for predicting survival of esophagogastric junction adenocarcinoma: a SEER population-based study and external validation. *BMC Gastroenterol* 2021; **21**: 38 [PMID: 33499821 DOI: 10.1186/s12876-021-01618-7]
3 **Xu H**, Zhang L, Miao J, Liu S, Liu H, Jia T, Zhang Q. Patterns of recurrence in adenocarcinoma of the esophagogastric junction: a retrospective study. *World J Surg Oncol* 2020; **18**: 144 [PMID: 32593312 DOI: 10.1186/s12957-020-01917-5]
4 **Ito H**, Inoue H, Odaka N, Satodate H, Suzuki M, Mukai S, Takehara Y, Kida H, Kudo SE. Clinicopathological characteristics and optimal management for esophagogastric junctional cancer; a single center retrospective cohort study. *J*

Exp Clin Cancer Res 2013; **32**: 2 [PMID: 23289488 DOI: 10.1186/1756-9966-32-2]

5 **Huang Q**. Carcinoma of the gastroesophageal junction in Chinese patients. *World J Gastroenterol* 2012; **18**: 7134-7140 [PMID: 23326117 DOI: 10.3748/wjg.v18.i48.7134]

6 **Giganti F**, Ambrosi A, Petrone MC, Canevari C, Chiari D, Salerno A, Arcidiacono PG, Nicoletti R, Albarello L, Mazza E, Gallivanone F, Gianolli L, Orsenigo E, Esposito A, Staudacher C, Del Maschio A, De Cobelli F. Prospective comparison of MR with diffusion-weighted imaging, endoscopic ultrasound, MDCT and positron emission tomography-CT in the pre-operative staging of oesophageal cancer: results from a pilot study. *Br J Radiol* 2016; **89**: 20160087 [PMID: 27767330 DOI: 10.1259/bjr.20160087]

7 **Soo TM**, Bernstein M, Provias J, Tasker R, Lozano A, Guha A. Failed stereotactic biopsy in a series of 518 cases. *Stereotact Funct Neurosurg* 1995; **64**: 183-196 [PMID: 8817805 DOI: 10.1159/000098747]

8 **Bhandari A**, Ibrahim M, Sharma C, Liong R, Gustafson S, Prior M. CT-based radiomics for differentiating renal tumours: a systematic review. *Abdom Radiol (NY)* 2021; **46**: 2052-2063 [PMID: 33136182 DOI: 10.1007/s00261-020-02832-9]

9 **Reginelli A**, Nardone V, Giacobbe G, Belfiore MP, Grassi R, Schettino F, Del Canto M, Cappabianca S. Radiomics as a New Frontier of Imaging for Cancer Prognosis: A Narrative Review. *Diagnostics (Basel)* 2021; **11** [PMID: 34679494 DOI: 10.3390/diagnostics11101796]

10 **Ibrahim A**, Primakov S, Beuque M, Woodruff HC, Halilaj I, Wu G, Refaee T, Granzier R, Widaatalla Y, Hustinx R, Mottaghy FM, Lambin P. Radiomics for precision medicine: Current challenges, future prospects, and the proposal of a new framework. *Methods* 2021; **188**: 20-29 [PMID: 32504782 DOI: 10.1016/j.ymeth.2020.05.022]

11 **Lambin P**, Leijenaar RTH, Deist TM, Peerlings J, de Jong EEC, van Timmeren J, Sanduleanu S, Larue RTHM, Even AJG, Jochems A, van Wijk Y, Woodruff H, van Soest J, Lustberg T, Roelofs E, van Elmpt W, Dekker A, Mottaghy FM, Wildberger JE, Walsh S. Radiomics: the bridge between medical imaging and personalized medicine. *Nat Rev Clin Oncol* 2017; **14**: 749-762 [PMID: 28975929 DOI: 10.1038/nrclinonc.2017.141]

12 **Scapicchio C**, Gabelloni M, Barucci A, Cioni D, Saba L, Neri E. A deep look into radiomics. *Radiol Med* 2021; **126**: 1296-1311 [PMID: 34213702 DOI: 10.1007/s11547-021-01389-x]

13 **Ren C**, Zhang J, Qi M, Zhang Y, Song S, Sun Y, Cheng J. Correction to: Machine learning based on clinico-biological features integrated 18F-FDG PET/CT radiomics for distinguishing squamous cell carcinoma from adenocarcinoma of lung. *Eur J Nucl Med Mol Imaging* 2021; **48**: 1696 [PMID: 33532911 DOI: 10.1007/s00259-021-05226-1]

14 **Tomori Y**, Yamashiro T, Tomita H, Tsubakimoto M, Ishigami K, Atsumi E, Murayama S. CT radiomics analysis of lung cancers: Differentiation of squamous cell carcinoma from adenocarcinoma, a correlative study with FDG uptake. *Eur J Radiol* 2020; **128**: 109032 [PMID: 32361604 DOI: 10.1016/j.ejrad.2020.109032]

15 **Zhao H**, Li W, Huang W, Yang Y, Shen W, Liang P, Gao J. Dual-Energy CT-Based Nomogram for Decoding HER2 Status in Patients With Gastric Cancer. *AJR Am J Roentgenol* 2021; **216**: 1539-1548 [PMID: 33852330 DOI: 10.2214/AJR.20.23528]

16 **Xu L**, Yang P, Yen EA, Wan Y, Jiang Y, Cao Z, Shen X, Wu Y, Wang J, Luo C, Niu T. A multi-organ cancer study of the classification performance using 2D and 3D image features in radiomics analysis. *Phys Med Biol* 2019; **64**: 215009 [PMID: 31561245 DOI: 10.1088/1361-6560/ab489f]

17 **Meng L**, Dong D, Chen X, Fang M, Wang R, Li J, Liu Z, Tian J. 2D and 3D CT Radiomic Features Performance Comparison in Characterization of Gastric Cancer: A Multi-Center Study. *IEEE J Biomed Health Inform* 2021; **25**: 755-763 [PMID: 32750940 DOI: 10.1109/JBHI.2020.3002805]

18 **Huang WP**, Liu SY, Han YJ, Li LM, Liang P, Gao JB. Development of CT-Based Imaging Signature for Preoperative Prediction of Invasive Behavior in Pancreatic Solid Pseudopapillary Neoplasm. *Front Oncol* 2021; **11**: 677814 [PMID: 34079766 DOI: 10.3389/fonc.2021.677814]

19 **Mackin D**, Fave X, Zhang L, Yang J, Jones AK, Ng CS, Court L. Harmonizing the pixel size in retrospective computed tomography radiomics studies. *PLoS One* 2017; **12**: e0178524 [PMID: 28934225 DOI: 10.1371/journal.pone.0178524]

20 **van Griethuysen JJM**, Fedorov A, Parmar C, Hosny A, Aucoin N, Narayan V, Beets-Tan RGH, Fillion-Robin JC, Pieper S, Aerts HJWL. Computational Radiomics System to Decode the Radiographic Phenotype. *Cancer Res* 2017; **77**: e104-e107 [PMID: 29092951 DOI: 10.1158/0008-5472.CAN-17-0339]

21 **Koo TK**, Li MY. A Guideline of Selecting and Reporting Intraclass Correlation Coefficients for Reliability Research. *J Chiropr Med* 2016; **15**: 155-163 [PMID: 27330520 DOI: 10.1016/j.jcm.2016.02.012]

22 **Daghir-Wojtkowiak E**, Wiczling P, Bocian S, Kubik Ł, Kośliński P, Buszewski B, Kaliszan R, Markuszewski MJ. Least absolute shrinkage and selection operator and dimensionality reduction techniques in quantitative structure retention relationship modeling of retention in hydrophilic interaction liquid chromatography. *J Chromatogr A* 2015; **1403**: 54-62 [PMID: 26037317 DOI: 10.1016/j.chroma.2015.05.025]

23 **Zhou Y**, Hou P, Zha K, Liu D, Wang F, Zhou K, Gao J. Spectral Computed Tomography for the Quantitative Assessment of Patients With Carcinoma of the Gastroesophageal Junction: Initial Differentiation Between a Diagnosis of Squamous Cell Carcinoma and Adenocarcinoma. *J Comput Assist Tomogr* 2019; **43**: 187-193 [PMID: 30371624 DOI: 10.1097/RCT.0000000000000826]

24 **Gao X**, Ma T, Cui J, Zhang Y, Wang L, Li H, Ye Z. A CT-based Radiomics Model for Prediction of Lymph Node Metastasis in Early Stage Gastric Cancer. *Acad Radiol* 2021; **28**: e155-e164 [PMID: 32507613 DOI: 10.1016/j.acra.2020.03.045]

25 **Qiang JW**, Zhou KR, Lu G, Wang Q, Ye XG, Xu ST, Tan LJ. The relationship between solitary pulmonary nodules and bronchi: multi-slice CT-pathological correlation. *Clin Radiol* 2004; **59**: 1121-1127 [PMID: 15556595 DOI: 10.1016/j.crad.2004.02.018]

Published by **Baishideng Publishing Group Inc**
7041 Koll Center Parkway, Suite 160, Pleasanton, CA 94566, USA
Telephone: +1-925-3991568
E-mail: bpgoffice@wjgnet.com
Help Desk: https://www.f6publishing.com/helpdesk
https://www.wjgnet.com